Fig. 2 shows the bit error probability variation of the coded schemes for different interleaver lengths N = 100, 1000 and 10000 in a SMC. Similarly, Figs. 3 and 4 show the error probability variations in a LMC channel and in a Gaussian channel, respectively. For comparison, the error rate variations of uncoded FSK with LDI detection when BT_b = 1 have also been plotted in Figs. 2 – 4. It is mentioned here that the parameters F_{Dm} and F_D in a Gaussian channel, and F_D in an LMC do not exist. It is seen from the numerical results that the coded scheme can perform significantly better than the uncoded scheme in all channels. It is seen from Figs. 2 and 3 that the error rate floor in a fading channel can be significantly lowered by using turbo codes. Note that the above gains can be achieved at the expense of bandwidth and complexity due to the addition of the code. Finally, comparing binary signalling with octonary signalling, it is seen that binary signalling performs better in all channels, but it requires a faster transmission rate.

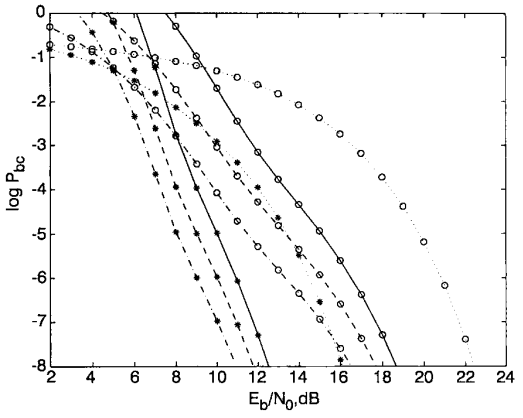

Fig. 4 *Bit error probability variation of the signalling schemes in a Gaussian channel*

——— N = 100
– – – – N = 1000
– · – · N = 10000
····· uncoded signalling
✳ binary signalling
O octonary signalling

Conclusions: Performance of turbo codes with FSK modulation and LDI detection have been analysed. Numerical results presented for Gaussian, land mobile and satellite mobile channels show that turbo codes can significantly improve the performance over uncoded signalling.

4 November 1998

Electronics Letters Online No: 19990098

J.P. Fonseka (*School of Engineering and Computer Science, EC 33, University of Texas at Dallas, 2601 N. Floyd Road, Richardson, TX 75080, USA*)

E-mail: kjp@utdallas.edu

References

1 BERROU, C., GLAVIEUX, A., and THITIMAJSHIRMA, P.: 'Near Shannon limit error correcting coding and decoding: turbo codes'. Proc. ICC, 1993, pp. 1064–1070

2 BENEDETTO, S., and MONTORSI, G.: 'Unveiling of turbo codes: Some results on parallel concatenated coding schemes', *IEEE Trans.*, 1996, **IT-42**, pp. 409–428

3 DIVSALAR, D., and POLLARA, F.: 'Turbo codes for PCS applications'. Proc. ICC, 1995, pp. 54–59

4 KORN, I.: 'M-ary frequency shift keying with limiter discriminator integrator detector in satellite mobile channel with narrowband receiver filter', *IEEE Trans.*, 1990, **COM-38**, pp. 1771–1778

5 LIN, S., and COSTELLO, J.: 'Error control coding: Fundamentals and applications' (Prentice Hall, 1983)

Automatic calibration of channels frequency response in interferometric radiometers

A. Camps, F. Torres, J. Bará, I. Corbella and F. Monzón

The large field of view required in Earth observation interferometric radiometers does not enable the use of a variable delay to compensate for different transit times, as in radioastronomy. A technique is presented to characterise the influence of a channels frequency response automatically in the shape of the cross-correlation function.

Introduction: When an interferometric radiometer (IR) images a large field of view, each pixel in the scene contributes with its own delay, which cannot be compensated for. The overall effect is a smoothing in the radial direction at the image edges, which constitutes a fundamental limitation of IR systems, if not corrected. A technique to characterise the cross-correlation (fringe-wash) function of each baseline so as to account for it in the inversion algorithm is presented here.

The basic measurement of an IR is the so-called visibility function V_{kj}, in Kelvin. This is obtained from the cross-correlation of the signals $b_k(t)$ and $b_j(t)$, collected by antennas k and j, which are located over the XY plane and spaced by a normalised distance $(u_{kj}, v_{kj}) = (x_j - x_k, y_j - y_k)/\lambda_0$. This is called the baseline [1].

$$V_{kj} = V(u_{kj}, v_{kj}) \triangleq \frac{1}{k_B\sqrt{B_k B_j}\sqrt{G_k G_j}} \cdot \frac{1}{2}\langle b_k(t) b_j^*(t)\rangle$$
$$\triangleq \frac{1}{\sqrt{\Omega_k \Omega_j}} \iint_{\xi^2+\eta^2\le 1} \frac{T_B(\xi,\eta)}{\sqrt{1-\xi^2-\eta^2}} F_{nk}(\xi,\eta) F_{nj}^*(\xi,\eta)$$
$$\times \tilde{r}_{kj}\left(-\frac{u_{kj}\xi + v_{kj}\eta}{f_0}\right) e^{-j2\pi(u_{kj}\xi + v_{kj}\eta)} d\xi d\eta \qquad (1)$$

where k_B is the Boltzmann constant, B_{kj} and G_{kj} are the noise bandwidth and the power gain of the receiving chains, Ω_{kj} and $F_{nk,j}(\xi,\eta)$ are the equivalent solid angle and the normalised radiation voltage patterns of the antennas, assumed to be located over the XY plane, and $(\xi,\eta) = (\sin\theta\cos\phi, \sin\theta\sin\phi)$ are the director cosines with respect to the X and Y axes respectively. $\tilde{r}_{kj}$ is the so-called fringe-wash function, which accounts for spatial decorrelation effects and depends on the frequency response of the normalised channels, $H_{nk,j}(f)$ through

$$\tilde{r}_{kj}(\tau) = \frac{e^{-j2\pi f_0 \tau}}{\sqrt{B_k B_j}} \int_0^\infty H_{nk}(f) H_{nj}^*(f) e^{j2\pi f\tau} df$$
$$= \frac{1}{\sqrt{B_k B_j}} F^{-1}[H_{nk}(f+f_0) H_{nj}^*(f+f_0) u(f+f_0)] \qquad (2)$$

with $f_0 = c/\lambda_0$ being an arbitrary centre frequency and $u(\ )$ the unity step function. Note that a change in the selection of f_0 (eqn. 2) produces a change in the slope of the phase of the fringe-wash function by an amount $e^{j2\pi\Delta f\tau}$. Note also that the brightness temperature $T_B(\xi,\eta)$ in eqn. 1 can be inverted by means of an inverse Fourier transform if: (i) the antenna voltage patterns are the same $F_{nk}(\xi,\eta) = F_{nj}(\xi,\eta)$, and (ii) the spatial decorrelation effects $\tilde{r}_j(\tau) \simeq 1$ are negligible. However, in planned Earth observation IRs (e.g. ESTAR or MIRAS), a large number of baselines must be simultaneously measured, and antenna voltage pattern and receiver frequency response mismatch are expected to be major error sources that have to be accurately accounted for in the inversion algorithms [2, 3]. Antenna patterns are expected to suffer minor variations during the life of a mission and can be on-ground characterised. On the other hand, the frequency responses of receivers are expected to vary with temperature drifts and aging of electronics, and the fringe-wash function (eqn. 2) must be periodically characterised.

X-band IR prototype: The measurement technique presented in this Letter is a new feature incorporated in the X-band IR recently developed at UPC [5]. The instrument consists of a pair of superheterodyne receivers that perform a two-step DSB coherent in-phase/quadrature down-conversion. Various operating modes are available, allowing different combinations of sampling rates (f_s =

66 and 80MHz) and half-power base-band bandwidths (B_{BB} = 10.7 and 21.4MHz, $B_{RF} = 2B_{BB}$). The complex cross-correlation is performed by means of a 1 bit/2 level (1B/2L) digital correlator integrated in a programmable logic device (model EPM MAX9400 LC-15 of Altera). The real and imaginary parts of the complex cross-correlation are, respectively, computed from the real cross-correlations of $i_1 - i_2$ and $i_1 - q_2$. The shape of $\tilde{r}(\tau)$ is measured from the cross-correlation of the signals with delayed versions of themselves, at steps given by the clock period. The sampled points are then interpolated by means of cubic spline functions for all possible delays $\tau = -(u_{kj}\,\xi + v_{kj}\,\eta)/f_0$ (eqn. 1). A low interpolation error is achieved by means of oversampling ($f_s > 2B$). Following the technique described in [4], at f_s = 80MHz the accuracy of the real and imaginary channels, respectively, is found to be better than 1% and 0.5% for time delays in the interval $|\tau| < 50$ns.

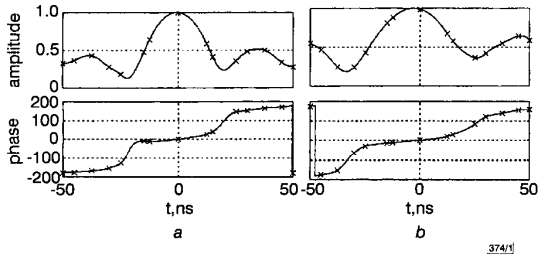

Fig. 1 *Measured fringe-wash function with 24.7 and 14.5MHz noise bandwidth LPFs*

a 24.7MHz
b 14.5MHz

Fringe-wash function characterisation: Setting the bandwidths at 10.7 and 21.4MHz, $\tilde{r}(\tau)$ was measured at 66 and 80MHz clock rates. The $\tilde{r}(\tau)$ functions interpolated from measurements at both f_s were more accurate than those interpolated from measurements at a single f_s, and were used as a reference to assess the error committed. According to numerical simulations, the accuracy improvement can be about a factor of 3 for the amplitude, and a factor of 10 for the phase. Results were then compared to the function interpolated by using only 66 or 80MHz sampled data.

Measurements are shown in Fig. 1*a* for the 21.4MHz and Fig. 1*b* for the 10.7MHz bandwidths. Note that:

(i) the smaller the bandwith, the wider the fringe-washing function, as expected from eqn. 2;

(ii) the equivalent noise bandwidth of the baseline can be derived from the position of the amplitude valleys: about 24.7 and 14.5MHz, larger than the half-power nominal bandwidths;

(iii) maximum amplitude is not at $\tau = 0$, due to different group delay frequency responses. It can be displaced by several nanoseconds;

(iv) the 180° phase step near the amplitude minima is not abrupt, due to the mismatch between $i_1 - i_2$ and $i_1 - q_2$ responses;

(v) the phase is not zero, but has a linear behaviour near the origin: $\phi(\tau) = 2\,\pi\,\Delta f\tau$.

This slope is due to an ambiguity in the definition of the centre frequency of the filters. In fact, regardless of the shape of the filters, the measurement of Δf can be used to define, unambiguously, the centre frequency of the baselines: $f'_0 = f_0 + \Delta f$, and thus compute more accurately the angular resolution of the instrument.

Table 1: Estimated errors from 66.66 or 80MHz data compared to 66.66 and 80MHz data for 24.7 and 14.5MHz noise bandwidth lowpass filters

	24.7MHz LPF				14.5MHz LPF			
	f_s = 66.66MHz		f_s = 80MHz		f_s = 66.66MHz		f_s = 80MHz	
	Amplitude	Phase	Amplitude	Phase	Amplitude	Phase	Amplitude	Phase
	%	deg	%	deg	%	deg	%	deg
Max. error	5.99	5.72	2.51	5.91	2.99	1.78	1.39	1.84
RMS error	3.91	3.11	1.62	1.86	1.58	0.88	**0.69**	**0.54**

Since the fringe-wash term appears to multiply the antenna radiation voltage patterns (eqn. 1), the achievement of a specified radiometric accuracy (ΔT) requires the same tolerances for the amplitude and phase of the fringe-wash function as those required for the antenna patterns: ~ 0.5% in amplitude and 0.5° in the phase [6]. Table 1 summarises the estimated errors from the former measurements, which decrease with increasing over-sampling ratios, leading to wider $\tilde{r}(\tau)$ and closer sampling points. Note that ΔT = 1K could only be met for the smallest noise bandwidth 14.5MHz, and the 80MHz clock rate (f_s/B = 5.5). At this point it is important to note that a reduction of a system's bandwidth by a factor of 2 produces a $\sqrt{2}$ = 1.41 radiometric sensitivity loss. This loss is partially compensated by oversampling and depends on the correlator's type: for 1B/2L digital correlators the gain factor is $\sqrt{2}.46/1.82 = 1.16$ [7].

Conclusions: This Letter has presented a new and accurate technique that allows on-board calibration of the impact on $\tilde{r}(\tau)$ of frequency response mismatches and drifts of receivers, due to thermal variations and/or aging. This technique allows an unambiguous definition of the centre frequency, regardless of filter shape, which improves the prediction of the angular resolution of these instruments. Also, noise bandwidth of the channels can be derived from the cross-correlation of each signal with itself, which can be used as a test of frequency response inter-similarity. The technologies and circuit topology of the correlator developed are covered by Spanish patent no. 9800896.

Acknowledgments: This work has been supported by the Spanish Comisión Interministerial de Ciencia y Tecnología under grant CICYT TIC 96/0879.

21 October 1998
Electronics Letters Online No: 19990125

A. Camps, F. Torres, J. Bará, I. Corbella and F. Monzón (*Department of Signal Theory and Communications, Universitat Politècnica de Catalunya, Campus Nord, Mòdul D4, c/Jordi Girona 1-3, 08034 Barcelona, Spain*)

References

1 THOMPSON A.R., MORAN, J.M., and SWENSON, G.W.: 'Interferometry and synthesis in radio astronomy' (John Wiley and Sons, 1986)

2 RUF, C.S., SWIFT, C.T., TANNER, A.B., and LEVINE, D.M.: 'Interferometric synthetic aperture radiometry for the remote sensing of the Earth', *IEEE Trans. Geosci. Remote Sens.*, 1988, **26**, (5), pp. 597 611

3 CAMPS, A., BARÁ, J., TORRES, F., and CORBELLA, I.: 'Extension of the CLEAN technique to the microwave imaging of continuous thermal sources by means of aperture synthesis radiometers', *Prog. Electromag. Res.*, 1998, **PIER 18**, pp. 67–83

4 CAMPS, A., TORRES, F., CORBELLA, I., BARÁ J., and SOLER, X.: 'Calibration and experimental results of a two-dimensional interferometric radiometer laboratory prototype', *Radio Sci.*, 1997, **32**, (5), pp. 1821–1832

5 CAMPS, A., TORRES, F., CORBELLA, I., BARÁ, J., and LLUCH, J.A.: 'Threshold and timing errors of 1 bit/2 level digital correlators in Earth observation synthetic aperture radiometry', *Electron. Lett.*, 1997, **33**, (9), pp. 812–814

6 CAMPS, A., BARÁ, J., TORRES, F., CORBELLA, I., and ROMEU, J.: 'Impact of antenna errors on the radiometric accuracy of large aperture synthesis radiometers. Study applied to MIRAS', *Radio Sci.*, 1997, **32**, (2), pp. 657-668

7 HAGEN, J.B., and FARLEY, D.T.: 'Digital-correlation techniques in radio science', *Radio Sci.*, 1973, **8**, (8–9), pp. 775–784